Environmental Research 232 (2023) 116331

Contents lists available at ScienceDirect

Environmental Research

journal homepage: www.elsevier.com/locate/envres

Performance of biochar mixed cement paste for removal of Cu, Pb and Zn from stormwater

Pamodithya Wijeyawardana [a,b], Nadeeshani Nanayakkara [b], David Law [a], Chamila Gunasekara [a], Anurudda Karunarathna [c], Biplob Kumar Pramanik [a,d,*]

[a] School of Engineering, RMIT University Melbourne, Australia
[b] Faculty of Engineering, University of Peradeniya, Sri Lanka
[c] Faculty of Agriculture, University of Peradeniya, Sri Lanka
[d] Water: Effective Technologies and Tools (WETT) Research Centre, RMIT University, Australia

ARTICLE INFO

Keywords:
Cement composite
Heavy metals
Adsorption
Biochar
Compressive strength
Kinetics

ABSTRACT

Using biochar as a partial replacement of Portland cement in cementitious materials is a promising solution to mitigate negative environmental impacts. However, current studies in available literature primarily focus on the mechanical properties of composites made with cementitious materials and biochar. Therefore, this paper reports the effects of the type of biochar, the percentage of biochar addition, and the particle size of the biochar on the removal efficiency of Cu, Pb, and Zn, as well as the effect of contact time on the removal efficiency of Cu, Pb, and Zn, along with the compressive strength. The peak intensities of OH^-, CO_3^{2-} and Calcium Silicate Hydrate (Ca–Si–H) peaks increase with increasing biochar addition levels, reflecting increased hydration product formation. The reduction of particle size of biochar causes the polymerization of the Ca–Si–H gel. However, no significant changes were observed in heavy metal removal, irrespective of the percentage of biochar addition, the particle size of biochar, or the type of biochar added to the cement paste. Adsorption capacities above 19 mg/g, 11 mg/g and 19 mg/g for Cu, Pb and Zn were recorded in all composites at an initial pH of 6.0. The Pseudo second order model best described the kinetics of the Cu, Pb, and Zn removal. The rate of adsorptive removal increases with the decrease in the density of the adsorbents. Over 40% of Cu and Zn were removed as carbonates and hydroxides through precipitation, whereas over 80% of Pb removal was via adsorption. Heavy metals bonded with OH^-, CO_3^{2-} and Ca–Si–H functional groups. The results demonstrate that biochar can be used as a cement replacement without negatively impacting heavy metal removal. However, neutralization of the high pH is needed before safe discharge.

1. Introduction

The rapid development of the urban infrastructure has caused pollutants such as nutrients, heavy metals and hydrocarbons to accumulate on impervious surfaces in the urban environment (Mullaney and Lucke, 2014; Wang et al., 2017; Gavric et al., 2019). With rainfall, these accumulated pollutants are mixed with runoff and conveyed to receiving water bodies (Wang et al., 2017). The resulting runoff is identified as a major contributor to the degrading of the water quality of the receiving water bodies (Zuraini et al., 2018; Sidhu et al., 2020). Therefore, in the urban environment, stormwater is a major non-point source pollutant (Zuraini et al., 2018; Sidhu et al., 2020). Hence, the focus on treating urban runoff for safe discharge has grown (Mullaney and Lucke, 2014). Heavy metals are one of the most critical pollutants present in stormwater runoff due to their toxicity, non-degradability and bioaccumulation (Ma et al., 2016; Sidhu et al., 2020). Even though several heavy metals act as essential micronutrients for life, they can be the source of severe poisoning (Saleh, 2015; Alhashimi and Aktas, 2017). Heavy metals accumulate in the tissues of animals and plants that are exposed (Duruibe et al., 2007; Tchounwou et al., 2012). Due to the low concentrations of heavy metals in urban runoff, the direct risk to humans from single heavy metals in urban stormwater is not significant, but it is of high concern to the safety of aquatic life in the receiving waters)(Ma et al., 2016). Significant concentrations of Cu, Cd, Cr, Ni, and Zn are found in stormwater quality analysis throughout the literature)(Reddy et al., 2014). The most common heavy metals in stormwater are Cu, Pb

* Corresponding author. School of Engineering, RMIT University Melbourne, Australia.
E-mail address: biplob.pramanik@rmit.edu.au (B.K. Pramanik).

https://doi.org/10.1016/j.envres.2023.116331
Received 11 March 2023; Received in revised form 2 June 2023; Accepted 3 June 2023
Available online 10 June 2023

Table 1
Cement biochar paste adsorbents mix designs.

Biochar type		Composite name	Cement (g)	Water (g)	Biochar (g)	Biochar/Cement (volume) (%)	Biochar/Cement (mass) (%)
No biochar		Cement-only	1236	557.5	0	0	0
Sawdust	Un-sieved biochar	5% SDBC-U	1175		3.36	5	0.19
		10% SDBC-U	1113		6.72	10	0.40
		20% SDBC-U	989		13.43	20	0.86
	Crushed and sieved biochar	5% SDBC-CS	1175		6.88	5	0.40
		10% SDBC-CS	1113		13.27	10	0.79
		20% SDBC-CS	989		27.53	20	1.75
Paddy husk	Un-sieved biochar	5% PHBC-U	1175		3.77	5	0.22
		10% PHBC-U	1113		7.54	10	0.45
		20% PHBC-U	989		15.07	20	0.97
	Crushed and sieved biochar	5% PHBC-CS	1175		11.17	5	0.64
		10% PHBC-CS	1113		22.35	10	1.32
		20% PHBC-CS	989		44.69	20	2.81

and Zn (Sakson et al., 2018; Kayhanian et al., 2019). The stormwater quality degrades due to the strong toxicity and mobility of Cu, Pb and Zn Ma et al. (2016). Additionally, Cu and Zn have also been identified as the preliminary cause of toxicity in stormwater and are also identified as priority pollutants by the USEP(4))Kayhanian et al., 2008; USEPA, 2014. The harmful effects of Cu ions in humans include harm to the brain, heart, skin and pancreas (Park et al., 2008, 2017). Lead toxicity results in kidney failure, damage to the nervous system and impaired muscle function(1))Efome et al., 2018a,b; Gu et al., 2021. Excessive amounts of Zn result in stomachache, dehydration, nausea, dizziness, and electrolyte imbalance in the body (Park et al., 2008).

The usage of adsorption, ion exchange, filtration, and redox reactions to treat heavy metals can be widely found in the literature (Batool et al., 2017). Considering these treatments adsorption is cheap, versatile, and convenient for large-scale heavy metal removal (Batool et al., 2017; Efome et al., 2018b). A carbon-rich solid, biochar is synthesized via thermal dilapidation of biomass subjected to an oxygen-limited setting which is known as pyrolysis (Inyang et al., 2015; Shen et al., 2017). Unique properties of biochar include a porous structure, specific surface area, and surface functional groups making it a good adsorbent material (Dai et al., 2019; Sun et al., 2019). Biochar synthesized from pyrolysis of algae, hardwood, softwood, tobacco stems, rice straw and rice husks has been successfully used for the removal of Cu, Pb and Zn (Poo et al., 2018; Zhao et al., 2020). Furthermore, biochar synthesized with mixed hardwoods achieved approximately 70% and 58% removal of Zn and Cu respectively (Chen et al., 2011). Additionally, Cu removal efficiency of above 95% had been observed when biochar was synthesized with farmyard manure, waste marine macro-algae and poultry manure biochar (Batool et al., 2017; Poo et al., 2018). The use of these widely available materials in biochar production helps to drive down costs and reduce the burden of disposal of those materials (Tan et al., 2015). Agricultural biomass is one of the most abundant renewable resources with the capacity to be turned into biochar (Dai et al., 2019). Paddy husk, also referred to as rice husk, is the by-product of the rice milling industry and is 20% *w/w* of the total paddy products (Kumar et al., 2021). The annual global production of rice husks totals around 80 million tons (Kumar et al., 2021). Sawdust is also a similar feedstock material that has the potential to be turned into biochar and is available in large quantities (Kumar et al., 2021). However, most biochar reported in the literature is prepared in controlled laboratory settings where muffle furnaces are utilized. This is a high-energy intensive process and only a very limited quantity of biochar can be made. Furthermore, European guidelines for the sustainable production of biochar state that pyrolytic gases produced during the pyrolysis process should be burned to supply energy to the pyrolysis process. Hence, the usage of industrially manufactured biochar is cleaner and a lower concentration of fine particles, hydrocarbons, carbon monoxide and greenhouse gas are emitted to the environment compared to lab-scale production of biochar (Dai et al., 2019).

Cement-based systems are used for in situ immobilization of heavy metals through stabilization/fixation, and sorption (Rasoulifard et al., 2016; Damrongsiri, 2017). However, cement production is considered one of the main sources of greenhouse gas emissions (Herath et al., 2020; Fernando et al., 2022). Therefore, using waste materials as cement replacement has gained significant attention recently (Fernando et al., 2022). However, the addition of waste biomass raises concerns since it can degrade due to the high alkalinity of cementitious materials (Maljaee et al., 2021a). Turning biomass into biochar and using it as cement replacement helps to overcome this issue (Maljaee et al., 2021a). The feasibility of using biochar as cement replacement materials have been studied in the past (Gupta et al., 2020; Tan et al., 2020; Wang et al., 2020; Gupta and Kashani, 2021). These studies have evaluated the effect of biochar addition on carbon sequestration, shrinkage, compressive strength, and permeability of composites made with cement and biochar. Furthermore, these studies have used biochar synthesized in controlled laboratory conditions using furnaces (Gupta et al., 2020; Tan et al., 2020; Wang et al., 2020; Gupta and Kashani, 2021).

However, the effect of biochar addition on the water treatment ability of cement paste has not yet been studied in the available literature. Additionally, compared to lab-scale produced biochar used in the available literature, this study uses biochar synthesized in an industrial-type double chamber draft-down pyrolysis reactor. Overall, this study aims to (i) investigate the mechanical and chemical properties of biochar-cement composite using characterization techniques such as scanning electron microscopy (SEM) with energy dispersive X-ray analysis (EDX), Fourier transform infrared spectroscopy (FTIR), and X-ray diffraction analysis (XRD); (ii) investigate adsorption ability of heavy metals on biochar-cement composites and determine the adsorption mechanisms.

2. Materials and methods

2.1. Reagents

Heavy metal stock solutions with a concentration of 1000 mg L^{-1} of Cu, Pb and Zn were made by dissolving copper (II) nitrate (Cu $(NO_3)_2{\cdot}3H_2O$) (Sigma Aldrich, USA), lead (II) nitrate ($Pb(NO_3)_2$) (Sigma Aldrich, USA) and zinc (II) nitrate, (Zn $(NO_3)_2{\cdot}6H_2O$) (Sigma Aldrich, USA) with a purity of more than 99% in distilled water. All adsorption experiments were carried out using synthetically made stormwater. For each adsorption test, new solutions of 10 mg L^{-1} of the heavy metals were made by diluting premade heavy metal stock solutions with distilled water. Dilution of concentrated (37%) hydrochloric acid (Sigma Aldrich, USA) was done with distilled water to make a 1 M HCl solution. For the preparation of 1 M NaOH solution, NaOH tablets (Daejung, Korea) having an assay of 97% were dissolved in distilled water. HNO_3 (Sigma Aldrich, USA) with an assay of 70% was used to acidify the filtered samples.

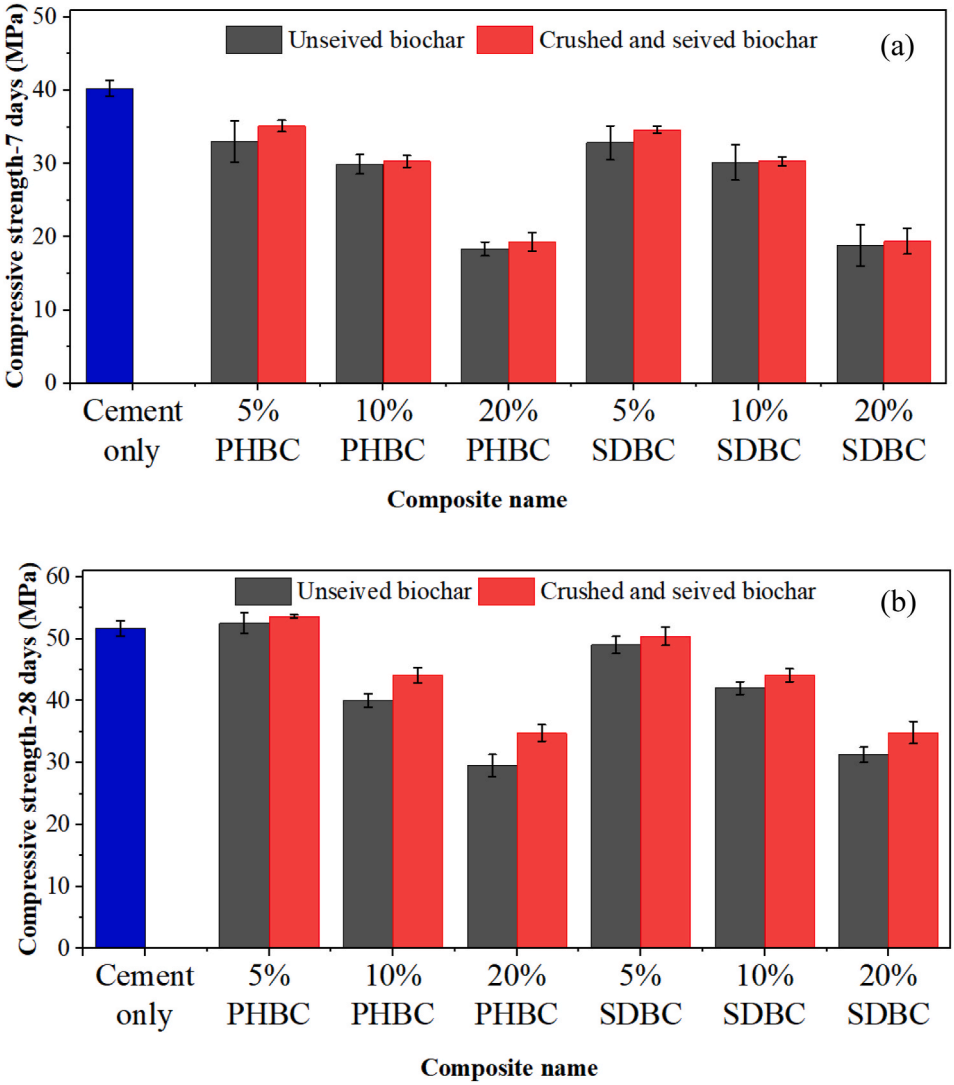

Fig. 1. Compressive strength of (a) 7 days and (b) 28 days cured composites.

2.2. Cement biochar paste

The biochar used in this study was prepared using a double chamber draft-down pyrolysis reactor with a residence time of 25 ± 5 min. Sawdust and paddy husk were used as feedstocks. Wijeyawardana et al. (2022b) found that pyrolysis temperatures of 350–450 °C and 450–550 °C for paddy husk and sawdust biochar respectively attained the highest removal of Cu, Pb and Zn. Hence, for this study paddy husk and sawdust biochar synthesized at pyrolysis temperatures of 350–450 °C and 450–550 °C respectively were applied. Ordinary Portland cement (Type I/II 32.5N) conforming to ASTM C150 was used, and biochar was added as a cement replacement in the range of 5–20% (*v/v*). A water/binder ratio of 0.45 was used for the control mix. The ingredients were mixed using an ASTM-compliant bench mixer (HOBART, USA). Initially, dry cement and biochar were mixed for 2 min at 139 rpm and then water was added. Thereafter, the mixing was continued for 1 min at 139 rpm and manually mixed for another 1 min. Then, the paste was mixed again at 139 rpm for another 2 min. The specimens were cast using cubic molds with a 50 mm × 50 mm cross-section and cured in saturated lime solution for 7 days. After the curing period, the compressive strength of the cubes was measured using a compressive strength testing machine (MATEST C070D, Italy) with a loading rate of 0.75 kN/s (AS 1012.9:2014). At least three replicates of the testing were done to obtain accurate results. The cured cement paste material was crushed, and oven dried for 24 h before sieving to isolate 4-2 mm range particles for usage in sorption experiments. Table 1 shows the mix design details of the cement pastes used. The base cement content used was 1230 kg m^{-3}.

2.3. Adsorption tests

Batch adsorption studies were done to evaluate the effect of biochar addition to cement paste adsorbents on Cu, Pb and Zn removal. 1000 mg L^{-1} copper nitrate, lead nitrate and zinc nitrate standard solutions were prepared and diluted to 10 mg L^{-1} for adsorption experiments. The solution pH was adjusted by adding hydrochloric acid or sodium hydroxide as required. From the prepared synthetic heavy metal solutions, 500 mL were decanted and placed in 750 mL high density polyethylene bottles and the weighed adsorbents were added. The adsorbent dosage used was 0.5 g L^{-1}. The samples were placed in a thermostatic reciprocating shaker set to 150 rpm for 24 h. After the desired time had passed, the solution was filtered using 0.45 μm filter papers and acidified with HNO_3 and final metal concentrations were measured unless stated otherwise. All the adsorption experiments were done at room temperature 25 ± 1.5 °C. equation (S1) for calculating removal efficiency of heavy metals is described in the supplementary information.

To understand the contribution of precipitation and sorption to the cement paste, the pH of the supernatant was adjusted using HNO_3

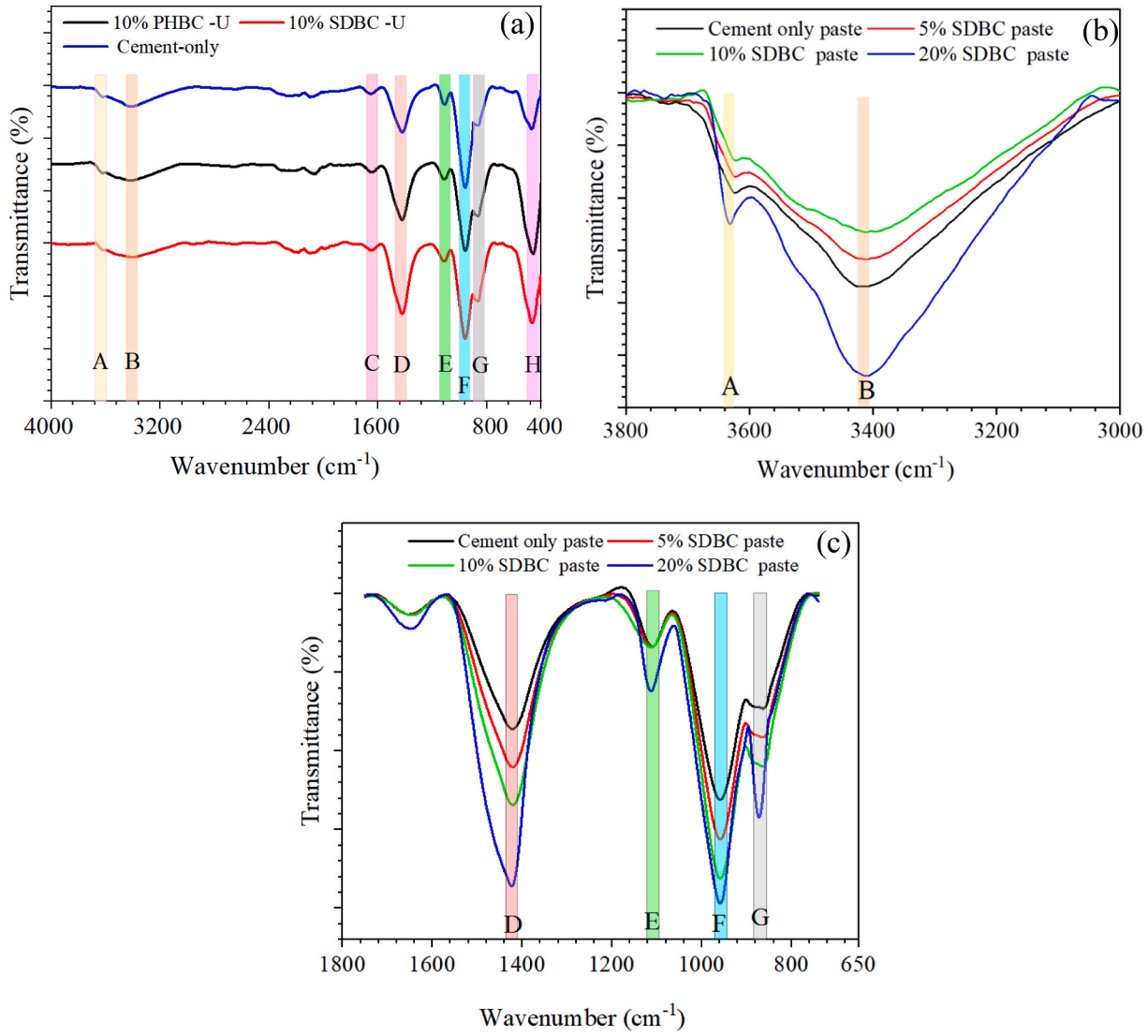

Fig. 2. FTIR of (a) cement-only, 10% unsieved paddy husk biochar mixed and 10% unsieved sawdust biochar mixed added, (b) peaks from 3800 to 2800 cm^{-1} (c) peaks from 1800 to 800 cm^{-1} of 7 days cured adsorbents.

(without affecting the concentration). Once the sorption experiment was concluded, a part of the supernatant was extracted and acidified such that the final pH was <2.0. This was filtered using 0.45 μm filter paper and the residual heavy metal concentration was measured. The characterization of the spent adsorbents was done by isolating the spent adsorbents after filtering the supernatants. The spent adsorbents were oven dried for 24 h at 105 °C. The spent adsorbents were analyzed using FTIR and XRD to identify any changes due to the sorption of heavy metals. All removal experiments were replicated at least three times to obtain accurate results. To examine the adsorption kinetics of Cu, Pb and Zn removal, Pseudo first order and Pseudo second order models were used. The linearized model equations (S2 and S3) are described in the supplementary information.

2.4. Analysis method

The pH values were measured by using a pH probe (pH probe; Orion 910003, U.S.A) connected to a multiparameter meter (Thermo Orion A325, USA). The surface functional groups of the PHBC and SDBC were determined by the Fourier transform infrared spectroscopy (UATR two; PerkinElmer, USA). A scanning electron microscope and energy dispersive spectrometer (EVO 18; ZEISS, Germany) was used to observe the microstructures and element compositions of PHBC and SDBC. The mineral compositions of the adsorbents were determined by X-ray Diffractometer (Bruker D8 Advance X-ray diffractometer, USA). An atomic absorption spectrometer (Shimadzu AA-7000, Japan) was used to measure concentrations of Cu, Pb and Zn in the solutions. Particle size analysis for unsieved biochar was undertaken following ASTM D6913/D6913M-17 single-set sieving. The particle size of crushed and sieved biochar was measured using a particle size analyzer (Fritsch - Analysette 22 Nano Tech, Germany) in wet mode. All analyses were replicated at least three times to obtain accurate results.

3. Results and discussion

3.1. Compressive strength of cement pastes

Compressive strength is the most commonly used test to characterize cement-based materials. Reduction in compressive strength was observed when biochar was added when comparing the 7 day compressive strength values with the control (Fig. 1(a)). This is in agreement with the observations made by Chen et al. (2020) and Ofori-Boadu et al. (2021). As the unsieved biochar used in this study has a particle size distribution similar to fine aggregates (Fig. S1(a)) the

biochar particles are expected to behave similarly. Hence, they create a weak interfacial zone between the hydrated cement and biochar particles (Gupta et al., 2020). The lower strength of this interfacial zone in the biochar-mixed pastes could be a reason for the lower compressive strengths of the biochar-mixed pastes (Gupta et al., 2018b). A further reason for the lack of strength development is attributed to the moist curing of the cement paste, which was also adopted by Chen et al. (2020). For biochar mortar, moist curing has been reported to neutralize the effect of biochar addition as it provides sufficient water for hydration (Maljaee et al., 2021a). Thus, the benefit of internal curing from the addition of biochar is eliminated. However, Ofori-Boadu et al. (2021) state that compressive strength reduction is due to less calcium-silicate hydrate production. Conversely, FTIR analysis (Fig. 2) in this study reveals that a higher quantity of hydration products was formed in the 7-day cured samples. A similar observation was made by Chen et al. (2020) and Akhtar and Sarmah (2018a) using sludge-derived biochar and pulp and paper mill sludge where FTIR showed increased intensities of Ca–Si–H peaks after biochar addition. The inhomogeneous presence of hydration products within biochar pores has been reported not to contribute to the compressive strength of the pastes (Akinyemi and Adesina, 2020). The SEM images (Figs. S3 and S4) show that hydration products there are present inside the pores of the biochar particles.

The compressive strength of the paste after the addition of crushed and sieved biochar is higher than the samples where unsieved biochar was added. However, the compressive strength was lower than that of the control mix even after the addition of crushed and sieved biochar. A similar observation was made by Yang et al. (2021) as well where 2% and 5% (*w/w*) cement replacement was undertaken utilizing commercial biochar with particle size less than approximately 800 μm compared to less than 75 μm (Fig. S1(b)) in this study. Comparing the mass percentages of biochar addition in this study, when crushed and sieved biochar is added, approximately twice the mass of cement can be replaced while achieving similar or higher strength than the addition of unsieved biochar at similar volume percentages of cement replacement. More than 90% of the unsieved biochar had particles ranging from 1 mm to 0.1 mm whereas crushed and sieved biochar had particles with a maximum size of 75 μm. It is hypothesized that crushed and sieved biochar is capable of creating a filler effect. This filler effect results in a denser paste thus improving the compressive strength (Gupta et al., 2020; Tan et al., 2020). Furthermore, the polymerization (shift in Ca–Si–H peak from 958 cm^{-1}) of the Ca–Si–H gel observed from FTIR analysis (section 3.2.1) also results in the compressive strength increase observed due to the addition of crushed and sieved biochar compared to samples with similar levels of cement replacement by volume using unsieved biochar (Maljaee et al., 2021a; Chen et al., 2022).

Comparing the results of unsieved PHBC and SDBC addition, at 5% (*v/v*) replacement of cement, PHBC-added samples gave higher compressive strength than SDBC-added samples. Less than 1.55% (*w/w*) (equivalent to 20% (*v/v*)) biochar (unsieved biochar) was added in this study. The pozzolanic activity of PHBC was found to be prominent at higher dosages (~4% (*w/w*)) of biochar addition in cement paste by Maljaee et al. (2021b). At higher levels of biochar addition (10% and 20% (*v/v*)), the SDBC samples show slightly higher (0.3–0.5 MPa) average compressive strength at 7 days. This is attributed to the particle size of SDBC being less than PHBC which creates a filler effect when SDBC is added (Tan et al., 2020; Maljaee et al., 2021a). It has been reported that the filler effect of biochar has a greater impact on strength than the pozzolanic reactivity of the biochar (Akhtar and Sarmah, 2018a). However, in this experiment when crushed and sieved biochar was used, this was not observed. This is attributed to the density of crushed and sieved PHBC (569.4 kg m^{-3}) being higher than SDBC (350.7 kg m^{-3}). Therefore, more cement was replaced for an equal volume of crushed and sieved PHBC when compared to SDBC. However, the similarity in compressive strengths noted when the same volumes of crushed and sieved PHBC and SDBC are added is likely due to the pozzolanic effect of PHBC compensating for the reduction in cement in the PHBC compared to the SDBC (Maljaee et al., 2021b).

Table 2
The major peaks identified in 7 days cured cement pastes (Chen et al., 2020; Praneeth et al., 2020; Ofori-Boadu et al., 2021; Yang et al., 2021).

Letter	Wavenumber (cm^{-1})	Functional group	Letter	Wavenumber (cm^{-1})	Functional group
A	3642–3637	O–H of Ca $(OH)_2$	E	1114–1105	SO_4^{-2} of Ettringite (AFt)
B	3420–3410	–OH or H_2O	F	965–955	Ca–Si–H
C	1650–1640	C═C and C═O	G	877–874	CO_3^{-2}
D	1426–1424	C–O of CO_3^{-2}	H	550–525	Si–O

The increase in curing time increased the compressive strength (Fig. 1(b)). At 5% PHBC addition, the compressive strength is about 2 MPa higher than that of the control. This is similar to the observation made in 7-day cured samples. Additionally, at higher levels of biochar addition (10% and 20% (*v/v*)), the SDBC samples showed higher (2–5 MPa) average compressive strength at 28 days compared to less than 0.5 MPa after 7 days of curing. This is evidence supporting the hypothesis that the filler effect of the biochar has a greater effect on strength than the pozzolanic reactivity of the biochar (Akhtar and Sarmah, 2018a).

3.2. Characterization of cement paste

3.2.1. Fourier-transform infrared spectra of cement paste

The different functional groups present in the 7-day cured adsorbents are shown in FTIR images in Fig. 2 (Wang and Liu, 2017). The major peaks identified in 7-day cured cement pastes are shown in Table 2 (Roy et al., 2017; Akhtar and Sarmah, 2018a, 2018b; Praneeth et al., 2020; Yang et al., 2021). Comparing biochar paste with control paste specimens no additional peaks are identified. A similar observation was made in previous studies (Roy et al., 2017; Akhtar and Sarmah, 2018a; Ahmad et al., 2020; Yang et al., 2021). Comparison of peak intensities of FTIR spectra allows qualitative comparison of the amount of respective functional groups (Wang and Liu, 2017; Zhou et al., 2018; Mbui et al., 2021). Peak intensity increment is an indicator of the presence of a higher concentration of the respective functional group (Shin et al., 1997; Chen et al., 2020). Comparing carbonate peaks, D and G, the intensities of the peaks are highest for PHBC followed by SDBC. The cement-only sample shows the lowest intensity of carbonation. A detailed comparison of the CaOH peak highlights that the cement-only sample has the greatest intensity while biochar-added pastes displayed lower intensities. This imparity in intensities is more prominent in PHBC mixed paste, where the CaOH peak is the lowest. This is likely due to carbonation with CO_2 present in biochar and the lower cement content of biochar-mixed pastes (Gupta and Kua, 2019b; Maljaee et al., 2021b). Despite the lower cement content, the higher intensity of the Ca–Si–H peak reflects a higher presence of Ca–Si–H in biochar-mixed cement pastes compared to the control. The PHBC shows slightly higher Ca–Si–H content (F) compared to SDBC paste which is likely due to the higher silica content contributing to pozzolanic reactions with PHBC (Roy et al., 2017; Maljaee et al., 2021b).

The intensity of the Ca–Si–H peak (F) increased with biochar addition (Fig. 2(c)). This is contrary to observations made by Yang et al. (2021) where a slight decrease in peak intensities of Ca–Si–H was observed. However, Yang et al. (2021) used higher biochar content (2% and 5% *w/w*) in their research compared to less than 3.6% (*w/w*) in this research. In addition, the source of biochar used is not disclosed in Yang et al. (2021) study. Therefore, the reduction of cement content and change in the type of biochar in Yang et al. (2021) may have resulted in the lowering of Ca–Si–H peaks.

Increased replacement of cement by biochar caused an increase in

the C–O peak (Fig. 2(c)). The increase in the C–O peak gives an indirect measurement of the carbonation depth, which increased with biochar addition (Praneeth et al., 2020). In the carbonation process, CO_2 dissolves in the pore solution as CO_3^{2-} when the pH is above 9.0. Carbonation results in portlandite being converted into $CaCO_3$ (Calcite). Calcite production results in volume expansion in the paste which can lead to debonding and micro-cracking in the paste Gupta et al. (2018b). Furthermore, due to carbonation, the pH value of the paste will reduce, thus promoting the corrosion of any steel reinforcement in the concrete (Poursaee, 2016). The pH value of the cement pore solution can be reduced to less than 9.0 due to carbonation (Šavija and Luković, 2016). However, the lowering of pH was not observed after the addition of biochar into the paste. This is likely due to the increased porosity of the pastes encouraging the dissolution of more portlandite in the paste. Thus, offsetting any pH changes due to carbonation.

When biochar is crushed and sieved at 75 μm is used as cement replacement the Ca–Si–H peaks shifted to 967 and 974 cm^{-1} at 10% and 20% biochar addition respectively, compared with 958 cm^{-1} in the cement-only sample. Also, the carbonation peaks at D and G reduced in intensity compared to unsieved biochar addition. This is attributed to the possible polymerization of the Ca–Si–H groups, as observed by Ofori-Boadu et al. (2021) and Chen et al. (2022). This polymerization results in the formation of a dense and stable Ca–Si–H gel when sieved biochar was added to the cement pastes (Chen et al., 2022). This would account for the compressive strength of the mixes with crushed and sieved biochar achieving higher strength than the unsieved biochar-added pastes (Fig. 1). Additionally, the formation of dense hydrated matrix results in lower permeability and thus reduces the degree of carbonation, correlating with the lower carbonation peak intensities observed.

The hydration reactions progress with the curing time in cement-based products. When the curing time increased to 28 days, an increase in peak intensities of O–H, CO_3^{2-}, and Ca–Si–H is observed (Fig. S8). As the hydration reactions progress more portlandite and Ca–Si–H are produced. The shifting of the Ca–Si–H peak was observed in both crushed and sieved and unsieved biochar specimens in 28-day cured samples which were also observed at 7-day of cured samples as well. This is attributed to the polymerization of Ca–Si–H. Additionally, the AFt peaks observed in the 7-day cured samples are not seen in the 28-day cured samples. This is due to the AFt reacting with the tricalcium aluminate in the cement paste and converting it to monosulfoaluminate.

3.2.2. Scanning electron microscopy analysis

The SEM analysis (Figs. S3 and S4) shows that hydrated cement particles have blocked some of the pores in the biochar particles. Furthermore, precipitation of hydration products (calcium hydroxide, ettringite and calcium carbonate crystals) on the surface of the biochar particles can also be observed. A similar observation had been made by Gupta et al. (2018b) and Gupta and Kua (2019a). Gupta et al. (2018b) state that the formation of Ca–Si–H gel, portlandite and ettringite inside pores of biochar is promoted by the moist environment inside the biochar particles. Furthermore, calcium carbonates are formed due to carbonation by adsorbed CO_2 in the biochar pores (Gupta et al., 2018b). However, the production of additional Ca–Si–H increases strength only when it is a part of the paste matrix and bonds biochar particles to the paste. Therefore, the Ca–Si–H depositions inside the biochar particles do not contribute to strength development (Gupta et al., 2018b).

SEM images (Figs. S3 and S4) show gaps at the interface of biochar particles and the hardened cement paste. These gaps at interfaces introduce more void zones in the paste, which is reflected by the lower hardened density of paste containing biochar, which in turn reduces the compressive strength (Fig. S2). Similar observations were made by Gupta et al. (2018b) who used biochar made from mixed wood sawdust carbonized at 300 °C. This suggests that biochar is weakly bonded to cement paste, which is possibly due to expansive carbonation around the biochar particles (Gupta et al., 2018b). The mechanical properties of cement composites are highly affected by the interfacial zone in composites and therefore, poor bonding results in a loss of mechanical strength (Gupta et al., 2018b). Comparing the crushed and sieved biochar samples with the unsieved biochar, a denser structure can be observed in the former. The gaps at biochar-cement paste interfaces are also seen to be reduced in magnitude. The finer particles are coated with hydration products creating a dense structure, which was also observed by Gupta et al. (2018a). This is also in line with the higher compressive strengths observed in crushed and sieved biochar-added pastes.

3.3. Heavy metal removal with cement biochar paste mixes

3.3.1. Effect of biochar addition

The cement paste adsorbents removed more than 95% of Cu and Zn whereas Pb removal was less than 60%. A similar observation (Cu and Zn removal >98% and Pb removal <76%) had been made by Chen et al. (2018) where lime was used to remove Cu, Pb and Zn ions. The removal efficiency results show that biochar addition has no significant effect on the removal of Cu, Pb, or Zn (Fig. 4 (a)). The same can be observed for the final pH and the electrical conductivity values (Fig. S5 (a) and (b)). Analysis of the pH variation between Cu, Pb and Zn removal is recorded in Fig. S5 (a), pH is the lowest for Cu removal compared with Pb and Zn removal. Cu and Zn form hydroxide precipitate at the final pH following adsorption (equation (1) and (2)). Hence, the removal of OH^- ions from the solution makes the pH value lower than that of Pb, which does not precipitate as hydroxide. Lead precipitates as lead hydroxide at pH levels below 10.0 (equation (3)). (Chen et al., 2018). When pH increases above pH 11.0 the lead hydroxide starts to dissolve as $Pb(OH)_3^-$ (equation (3)) (Yoshida et al., 2003; Chen et al., 2018). At the final electrical conductivity of the effluent (Fig. S5 (b)) more ions are found in the effluent with Pb than Cu or Zn. The $Pb(OH)_3^-$ ions in the supernatant are re-converted to Pb^{2+} when the filtered supernatant is acidified before the measurement of concentration. Thus, the higher concentration of Pb ions in the effluent results in higher electrical conductivity of the effluent. Comparatively to Pb removal, the electrical conductivity in Cu and Zn effluents is slightly lower due to the higher removal of the respective ions from the solution.

$$Cu^{2+}{}_{(aq)} + Ca(OH)_{2(aq)} \rightarrow Cu(OH)_{2(s)} + Ca^{2+}_{(aq)} \quad (1)$$

$$Zn^{2+}{}_{(aq)} + Ca(OH)_{2(aq)} \rightarrow Zn(OH)_{2(s)} + Ca^{2+}_{(aq)} \quad (2)$$

$$Pb^{2+}_{(aq)} + Ca(OH)_{2(aq)} \rightarrow Pb(OH)_{2(s)} + Ca^{2+}_{(aq)} \quad (3)$$

$$Pb(OH)_{2(s)} + OH^-_{(aq)} \rightleftharpoons Pb(OH)^-_{3(aq)} \quad (4)$$

The variation in removal efficiency when the supernatants of Cu, Pb and Zn removal are acidified vs non-acidified before filtering (Fig. S6) shows that in acidified supernatant, the removal of Cu and Zn is approximately <50%. Therefore, it can be concluded that the majority (>50%) of the removal of Cu and Zn occurs due to the precipitation of Cu and Zn in the solution (equation (1) and (2)). On the other hand, for Pb removal, the removal via precipitation is negligible (<5%). This suggests that Pb removal occurs due to the sorption of Pb onto the cement paste. As most of the removal (>50%) of Cu and Zn happens via solution precipitation, subsequent acidification (i.e., mixing with acidic sources) of the treated water will release Cu and Zn. Therefore, it is important to have a filtering mechanism to prevent the passage of the Cu and Zn precipitates, but this is not needed for Pb ions as removal by precipitation is negligible.

3.3.2. Effect of crushed and sieved biochar addition and curing time

The smaller particle size of biochar has resulted in a denser paste. Hence, the porosity of the mix is reduced. The results of removal efficiencies for crushed and sieved biochar (Fig. 5) showed no significant change in removal efficiency. The density of the adsorbents increases when crushed and sieved biochar is added compared to unseived

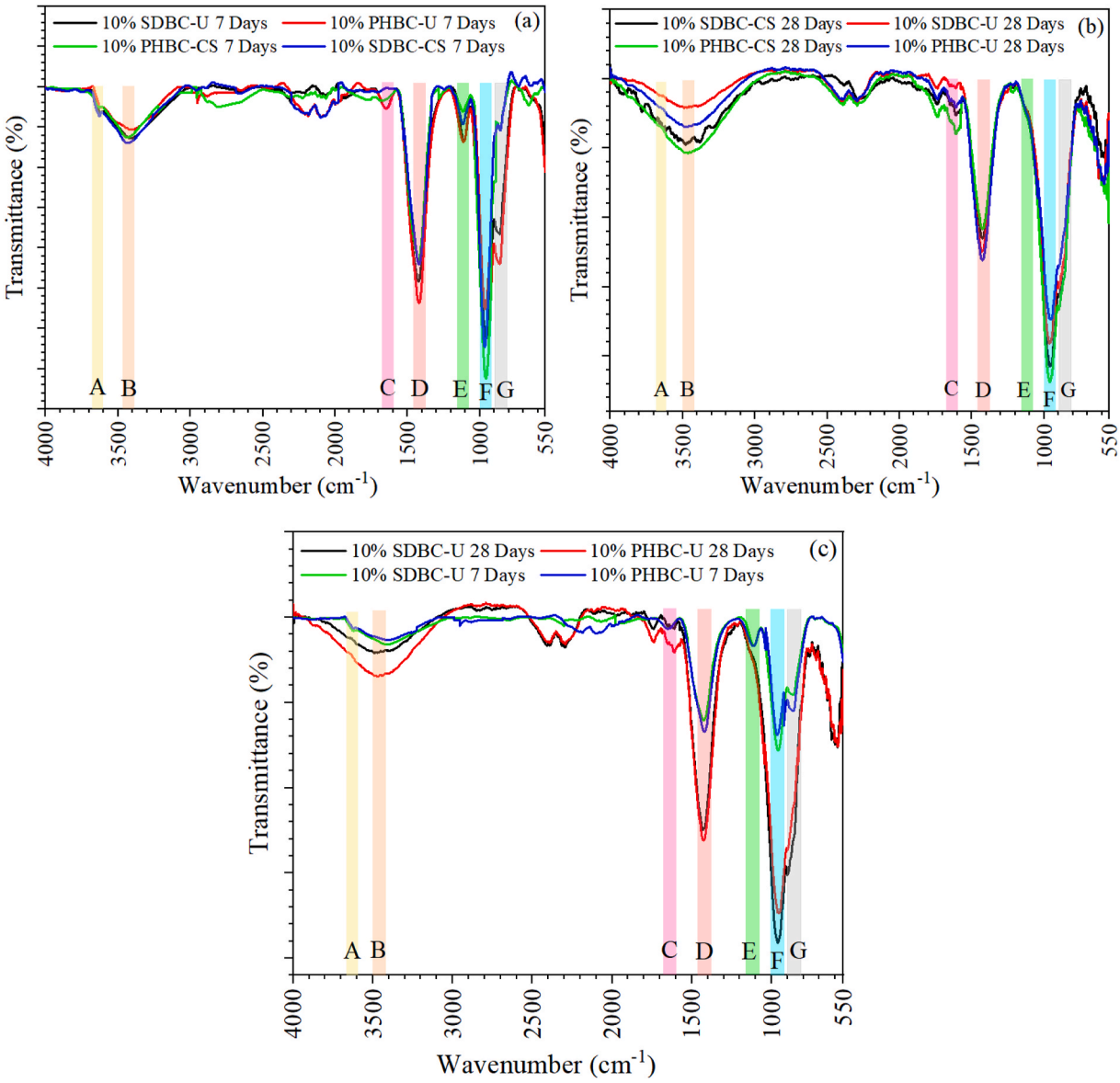

Fig. 3. FTIR of (a) 7 days cured, (b) 7 days vs 28 days cured and (c) 28 days cured composites with unsieved biochar/crushed and sieved biochar added.

biochar addition (Fig. S2). This phenomenon is reflected through the reduction of the peak intensity of the CO_3^{2-} peak with the addition of crushed and sieved biochar compared with the addition of unseived biochar. When the density of the cement paste is increased it reduces the diffusion of CO_2 into the cement paste adsorbent (Atis, 2004). Hence, although the biochar particle size is reduced, it has not enabled more diffusion pathways for the pollutants. Furthermore, the final pH value after adsorption is similar to when unsieved biochar was added, and the FTIR analysis (Fig. 3) does not indicate significant changes to intensity in Ca–Si–H, OH^- and Si–O functional groups. Hence, the overall removal of the three heavy metals remained unchanged when the biochar is crushed and sieved before being added.

The results of removal efficiencies for 28 days-cured samples (Fig. 4 (b)) showed no significant change in removal efficiencies compared with 7 days-cured samples. This is primarily due to the pH of the effluents being similar to that of 7 days cured samples. Furthermore, comparing the FTIR spectra of used 28 days cured adsorbents (Fig. S8) and 7 days cured adsorbents (Fig. 6), during the adsorptive removal, Cu, Pb and Zn ions interacted with similar functional groups. Hence, their absence of change in the removal efficiencies with curing time is justifiable as the removal mechanisms have not changed due to the curing time.

3.3.3. *Kinetics of Cu, Pb and Zn removal*

For the same pollutant, similar equilibrium contact times are observed for all three cement-only, 10% PHBC-U and 10% SDBC-U adsorbents (Fig. S7). The rate of metal sorption is assumed to be proportional to the number of unoccupied sites in Pseudo first order and Pseudo second-order models. Table 3 shows the summary of correlation efficiencies R^2 for Pseudo first order and Pseudo second order models and model parameters. The Pseudo second order model best fits the adsorption data. Hence, the sorption of all three heavy metals by the cement paste adsorbents is identified as chemisorption, which involves valence force sharing or electron exchange between the active sites of the adsorbent (Xu et al., 2021). The adsorption rate constant can be used to idealize the speed of adsorption of an adsorbate to an adsorbent (Chen et al., 2011). From the adsorption rate constants, Pb adsorbs more quicker than Cu and Zn despite the higher removal efficiencies observed for Cu and Zn removal. Also, heavy metal adsorption rates are in the order of 10% PHBC-U > 10% SDBC-U > cement-only. The removal rates correspond to the densities of the adsorbents where density increases 10% PHBC-U < 10% SDBC-U < cement-only. Thus, the lower density 10% PHBC-U paste allows the heavy metals to get adsorbed quicker than the higher dense 10% SDBC-U and cement-only sorbents.

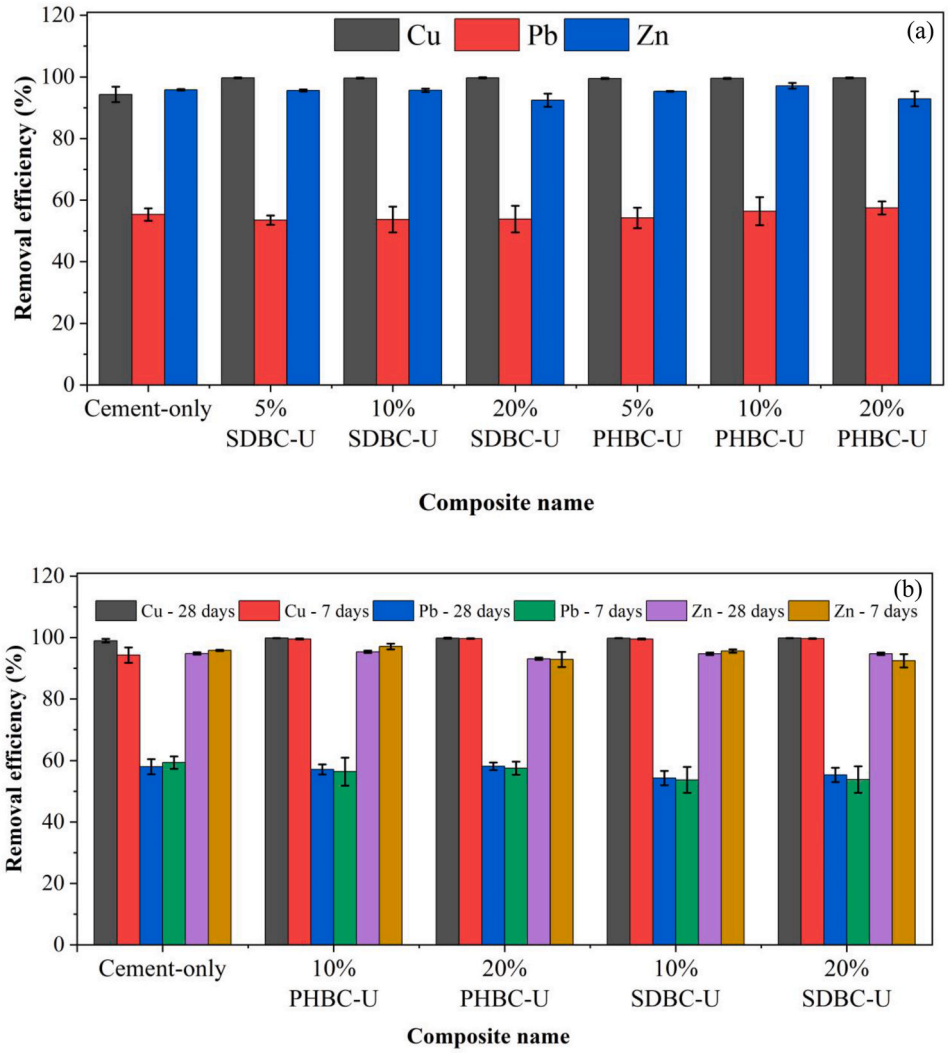

Fig. 4. Variation of removal efficiency of Cu, Pb and Zn removal with biochar addition levels for (a) 7 days cured and (b) 7 vs. 28 days cured composites (Temperature = 25 °C; initial pH = 6.0; adsorbent dosage = 0.5 g L^{-1}; initial Cu, Pb and Zn concentration = 10 mg L^{-1}).

3.3.4. *Removal mechanisms*

The FTIR and XRD spectra of the heavy metals post-adsorption are compared with pre-adsorption specimens to develop an understanding of the mechanisms of the process of removal of heavy metals (Yankovych et al., 2021). Compared to the control paste (cement-only adsorbent), the biochar-mixed adsorbents behaved similarly (Fig. S8). Comparing adsorbents used for heavy metal removal with the adsorbents in distilled water, major changes were observed in O–H, CO_3^{2-} and Ca–Si–H intensities. The intensities of these peaks were reduced after Cu, Pb and Zn removal. The intensity of this reduction suggests that these functional groups have contributed to the fixing of Cu, Pb and Zn (Qi et al., 2018; Zhou et al., 2018; Pan et al., 2019). In both cement-only paste and PHBC-mixed paste, the intensities of the hydroxides and carbonate peaks are reduced after Cu and Zn removal. This correlates with results in Fig. S6 where removal of Cu and Zn was primarily ascribed to precipitation whereas Pb removal via precipitation was low. The reduction of both hydroxide and carbonate peaks suggests the precipitation of heavy metal hydroxides and carbonates. Furthermore, Kumara et al. (2019) and Cheng et al. (2022) state that heavy metal removal in cementitious materials occurs via the substitution of Ca in Ca–Si–H by heavy metal ions (Fig. 6). This study supports this mechanism as Ca–Si–H peak intensity was reduced in post-adsorbents. The SO_4^{2-} peak disappeared in adsorbents placed in distilled water and utilized for Cu, Pb and Zn removal, suggesting that AFt has dissolved in the solution. The same observation was made for the $Ca(OH)_2$ peak which disappeared in adsorbents placed in distilled water and used for Cu, Pb and Zn removal. The rise of pH (to 11.0) after all adsorption experiments (after a contact time of 24 h) is due to the dissolution of $Ca(OH)_2$. When the curing time was increased to 28 days, an increase in peak intensities of O–H, CO_3^{2-}, and Ca–Si–H can be observed (Fig. S9). The heavy metals interacted with the functional groups (O–H, CO_3^{2-}, and Ca–Si–H) as the intensities of the peaks reduced after the adsorption())Qi et al., 2018; Pan et al., 2019.

Analysis of XRD data (Fig. S10) identified four major crystalline phases, calcium carbonate ($CaCO_3$), silica (SiO_2), calcium hydroxide ($Ca(OH)_2$), and ettringite. The XRD data of the surface layer of adsorbents used for heavy metal removal were compared with sorbents placed in distilled water to identify the precipitates on the surface of the adsorbents following heavy metal removal. Weak peaks corresponding to carbonates and hydroxides of Cu, Pb and Zn are observed in the XRD images. These results confirm the presence of heavy metal precipitates, as shown in Eqs (4)–(7). A similar observation has been made in available literature where granular hydrated Portland cement was used as an adsorbent (Cheng et al., 2022). The intensities of $CaCO_3$ peaks are slightly higher in biochar-added pastes than in the cement-only sample. Increased carbonation due to the addition of biochar to the adsorbents has resulted in these higher carbonate peaks compared with cement-only adsorbents (Qin et al., 2021). In addition, the $CaCO_3$ peak is

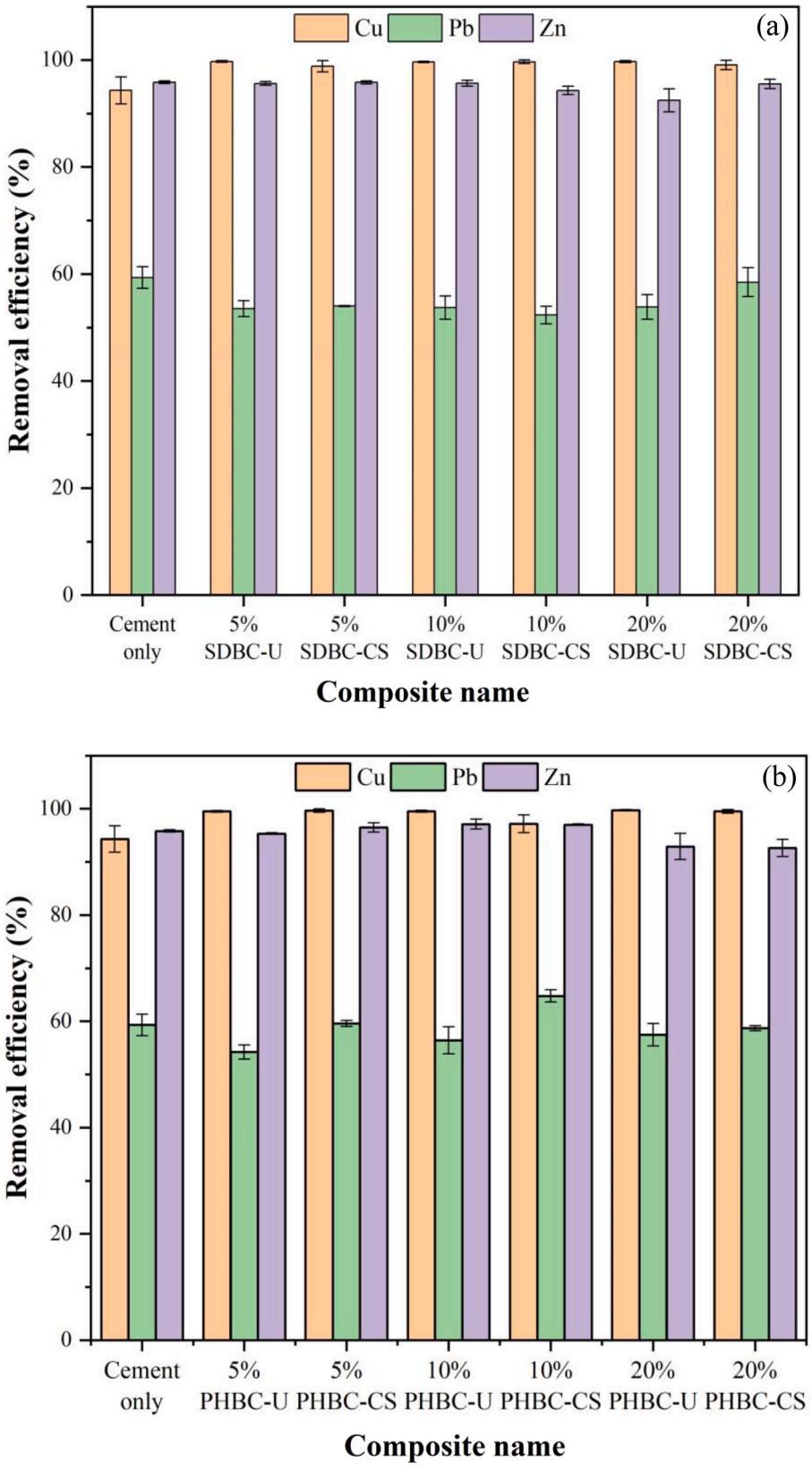

Fig. 5. Removal efficiency comparison of 7 days cured composite after the addition of crushed and sieved (a) sawdust and (b) paddy husk biochar.

higher than the $Ca(OH)_2$ peaks in all the samples. This is due to the dissolution of the $Ca(OH)_2$ when the adsorbents are placed in water (Cheng et al., 2022).

3.3.5. Characteristics of the effluent and reusability

There is an increment of Ca^{2+} ion concentration in the supernatant post-adsorption compared to when the adsorbent is initially put into the distilled water (Fig. S11). This shows evidence of Ca^{2+} ion leaching from

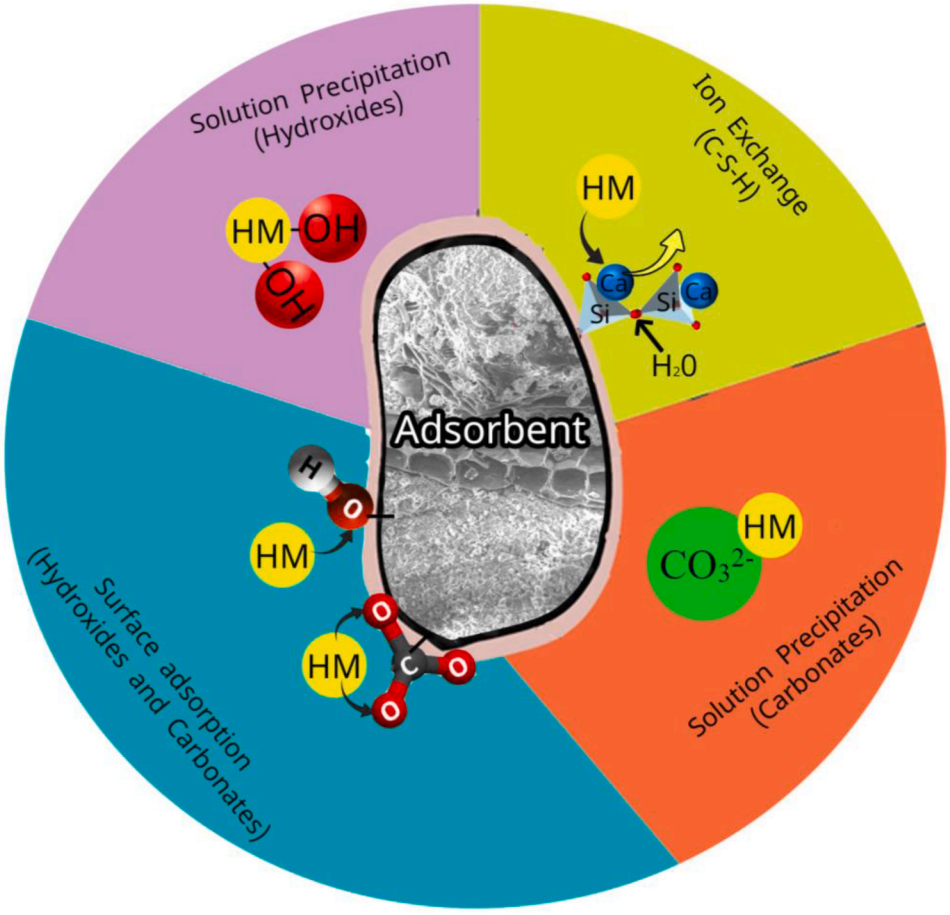

Fig. 6. Adsorption mechanisms of heavy metal removal with cement-biochar composite adsorbents.

Table 3
Results of adsorption kinetic modeling for Cu, Pb and Zn adsorption by adsorbent materials.

Adsorbent	Heavy metal	Pseudo first order model		Pseudo second order model	
		K_1 (min^{-1}) x 10^{-3}	R^2	K_2 (g. $mg^{-1}min^{-1}$) x 10^{-3}	R^2
Cement-only	Cu	13.7	0.9893	0.82	0.9902
	Pb	24.3	0.9441	1.25	0.9605
	Zn	15.9	0.9948	0.90	0.9955
10% PHBC-U	Cu	10.1	0.9577	1.05	0.9940
	Pb	23.9	0.9420	1.58	0.9632
	Zn	13.9	0.9884	0.95	0.9961
10% SDBC-U	Cu	10.1	0.9614	0.98	0.9939
	Pb	27.0	0.8686	1.28	0.9624
	Zn	44.6	0.9846	0.91	0.9944

the cement pastes when adsorption of Cu, Pb and Zn is occurring. The heavy metal hydroxide formation (Eq (4)) and the ion exchange between heavy metal and Ca in Ca–Si–H gel (Fig. 6) increase the Ca^{2+} ion concentration in the post-adsorption effluent. In similar research carried out using granular hydrated Portland cement, a positive correlation (R^2>*0.85*) was found between released Ca^{2+} and the removal capacity of Cu, Pb and Zn (Cheng et al., 2022). In comparison to Cu and Zn, Pb removal results in slightly lower Ca^{2+} ion concertation in the solution. This could be due to the lower removal rate of Pb which results in the displacement of fewer Ca^{2+} ions from the adsorbent material. The lower dry density of biochar adsorbents (Fig. S2) reflects that the addition of biochar increases the porosity of the paste (adsorbents). Thus, the

Table 4
Summary of adsorption capacities of common adsorbent materials in the removal of heavy metals.

Adsorbent material	Cu removal capacity (mg g^{-1})	Pb removal capacity (mg g^{-1})	Zn removal capacity (mg g^{-1})	Reference
Zeolite-modified Portland cement	23.25	27.03	12.85	Ok et al. (2007)
Iron-coated zeolite	9.33	11.6	6.22	Nguyen et al. (2015)
Apricot stone-activated carbon	24.08	22.84	–	Bohli et al. (2015)
Sulphurised activated carbon	–	–	12.3	Krishnan et al. (2016)
Apple tree branch biochar	11.41	–	10.22	Zhao et al. (2020)
Granular hydrated Portland cement	87.14	132.27	112.0	Cheng et al. (2022)
Rice husk biochar (Pyrolyzed at 350–450 °C)	6.89	17.57	2.64	Wijeyawardana et al. (2022a)
Sawdust biochar (Pyrolyzed at 450–550 °C	10.27	14.20	6.48	Wijeyawardana et al. (2022)
Cement-biochar composite	19.8	11.0	19.0	This study

concentration difference of Ca^{2+} ions in control and biochar cement pastes is due to the increase in porosity of the cement pastes, which results in an increased level of water permeability into the adsorbent (Gupta et al., 2020). Thereby, more ions leach from the cement pastes adsorbents. Despite the high removal efficiencies of Cu and Zn the effluent concentrations of Cu, Pb and Zn are in the range of 0.1–0.2 mg L^{-1}, 4–5 mg L^{-1} and 0.5–0.7 mg L^{-1} respectively. However, for safe discharge into receiving waterways with aquatic life, the Pb and Zn concentrations should be less than 0.065 mg L^{-1} and 0.120 mg L^{-1} respectively. Hence, the effluent requires further treatment before it can be safely discharged into receiving waterways. In addition, final pH values are greater than 11.0 and therefore the effluent pH should also be neutralized before discharge.

After used adsorbents were put in low-pH solutions, the adsorbed heavy metals starts to leach out below pH of 2.0 (Fig. S12). However, Pb leaching is more than 50% lower than that of Cu and Zn. As Cu and Zn removal was mainly via hydroxide precipitation, the acidic inflow is capable of dissolving the surface precipitates of Cu and Zn. Since Pb removal was mainly via adsorption, the desorption is lesser than that of Cu and Zn. Therefore, the adsorbent has the potential to be reused for Cu and Zn removal after being back washed with low pH (pH < 2.0) water.

4. Practical applications and future research prospects

The results of this research open new pathways to use biochar-modified cement paste in the treatment of heavy metal-laden stormwater. The cement-biochar adsorbents have similar adsorption capacities (Table 4) compared to commonly used adsorbents like zeolites, biochar and activated carbon. Hence, cement-biochar adsorbents can be used as an alternative absorbent in treatment units using commonly available adsorbents, especially for Cu and Zn removal. Additionally, as the effluent pH is high (pH > 11.0), it can be used to aid the removal of dissolved heavy metals from sources like acid mine drainage (Cravotta and Trahan, 1999). Furthermore, since the removed heavy metals are not washed off unless pH < 2.0, the used adsorbents synthesized in this study can be disposed of in acidic environments (6.0 > pH > 2.0) as well. To enhance the usefulness of the cement-biochar adsorbents, future research should consider evaluating the effect of competing ions, column removal efficiency, reusability of the adsorbents and methods of disposal of saturated adsorbents. Furthermore, testing and treatment of different wastewater streams should be done to broaden the usability of the adsorbents.

5. Conclusions

Biochar behaves as a filler material in biochar cement composites. Biochar addition does not significantly affect the Cu, Pb and Zn removal capacity of the cement paste due to effluent pH being similar. When the particle size of the biochar added was reduced, polymerization of Ca–Si–H gel occurs and decreases the density of the adsorbent. Chemisorption was the main mechanism of removal. Cu and Zn were mainly removed via precipitation while Pb was mainly removed via surface adsorption. Cu, Pb and Zn have interacted with the O–H, CO_3^{2-} and Ca–Si–H functional groups. Overall, all the adsorbents used showed adsorption capacities above 19 mg/g, 11 mg/g and 19 mg/g for Cu, Pb and Zn removal. Backwashing the adsorbents with high acidic (pH < 2.0) inflow causes the surface precipitated heavy metals to leach out. However, since the effluent pH is higher than 11.0 pH adjustment is required before safe discharge.

Credit author statement

Pamodithya Wijeyawardana: Data curation, Formal analysis, Experiment, Investigation, Methodology, Validation, Writing – original draft. Nadeeshani Nanayakkara: Conceptualization, Supervision, Writing – review & editing. Chamila Gunasekara: Conceptualization, Supervision, Writing – review & editing. David Law: Supervision, Writing – review & editing. Anurudda Karunarathna: Supervision, Writing – review & editing. Biplob Kumar Pramanik: Conceptualization, Project administration, Supervision, Writing – review & editing.

Declaration of competing interest

The authors declare that they have no known competing financial interests or personal relationships that could have appeared to influence the work reported in this paper.

Data availability

No data was used for the research described in the article.

Acknowledgments

The authors would like to thank RMIT University, Australia and the University of Peradeniya, Sri Lanka for the financial support.

Appendix A. Supplementary data

Supplementary data to this article can be found online at https://doi.org/10.1016/j.envres.2023.116331.

References

Ahmad, M.R., Chen, B., Duan, H., 2020. Improvement effect of pyrolyzed agro-food biochar on the properties of magnesium phosphate cement. Sci. Total Environ. 718, 137422.
Akhtar, A., Sarmah, A.K., 2018a. Novel biochar-concrete composites: manufacturing, characterization and evaluation of the mechanical properties. Sci. Total Environ. 616–617, 408–416.
Akhtar, A., Sarmah, A.K., 2018b. Strength improvement of recycled aggregate concrete through silicon rich char derived from organic waste. J. Clean. Prod. 196, 411–423.
Akinyemi, B.A., Adesina, A., 2020. Recent advancements in the use of biochar for cementitious applications: a review. J. Build. Eng. 32, 101705.
Alhashimi, H.A., Aktas, C.B., 2017. Life cycle environmental and economic performance of biochar compared with activated carbon: a meta-analysis. Resour. Conserv. Recycl. 118, 13–26.
Atis, C.D., 2004. Carbonation-porosity-strength model for fly ash concrete. J. Mater. Civ. Eng. 16, 91–94.
Batool, S., Idrees, M., Hussain, Q., Kong, J., 2017. Adsorption of copper (II) by using derived-farmyard and poultry manure biochars: efficiency and mechanism. Chem. Phys. Lett. 689, 190–198.
Bohli, T., Ouederni, A., Fiol, N., Villaescusa, I., 2015. Evaluation of an activated carbon from olive stones used as an adsorbent for heavy metal removal from aqueous phases. C. R. Chim. 18, 88–99.
Chen, L., Zhang, Y., Wang, L., Ruan, S., Chen, J., Li, H., Yang, J., Mechtcherine, V., Tsang, D.C.W., 2022. Biochar-augmented carbon-negative concrete. Chem. Eng. J. 431, 133946.
Chen, Q., Yao, Y., Li, X., Lu, J., Zhou, J., Huang, Z., 2018. Comparison of heavy metal removals from aqueous solutions by chemical precipitation and characteristics of precipitates. J. Water Process Eng. 26, 289–300.
Chen, X., Chen, G., Chen, L., Chen, Y., Lehmann, J., Mcbride, M.B., Hay, A.G., 2011. Adsorption of copper and zinc by biochars produced from pyrolysis of hardwood and corn straw in aqueous solution. Bioresour. Technol. 102, 8877–8884.
Chen, X., Li, J., Xue, Q., Huang, X., Liu, L., Poon, C.S., 2020. Sludge biochar as a green additive in cement-based composites: mechanical properties and hydration kinetics. Construct. Build. Mater. 262, 120723.
Cheng, P., Ren, Y., Yang, L., Li, R., Wang, X., Li, B., Yuan, H., 2022. Heavy metal removal from aqueous solution by granular hydrated Portland cement. Kor. J. Chem. Eng. 39, 3350–3360.
Cravotta, C.A., Trahan, M.K., 1999. Limestone drains to increase pH and remove dissolved metals from acidic mine drainage. Appl. Geochem. 14, 581–606.
Dai, Y., Zhang, N., Xing, C., Cui, Q., Sun, Q., 2019. The adsorption, regeneration and engineering applications of biochar for removal organic pollutants: a review. Chemosphere 223, 12–27.
Damrongsiri, S., 2017. Feasibility of using demolition waste as an alternative heavy metal immobilizing agent. J. Environ. Manag. 192, 197–202.
Duruibe, J.O., Ogwuegbu, M.O.C., Egwurugwu, J.N., 2007. Heavy metal pollution and human biotoxic effects. Int. J. Phys. Sci. 2, 112–118.
Efome, J.E., Rana, D., Matsuura, T., Lan, C.Q., 2018a. Insight studies on metal-organic framework nanofibrous membrane adsorption and activation for heavy metal ions removal from aqueous solution. ACS Appl. Mater. Interfaces 10, 18619–18629.
Efome, JE., Rana, D., Matsuura, T., Lan, C.Q., 2018b. Metal–organic frameworks supported on nanofibers to remove heavy metals. J. Mater. Chem. 6, 4550–4555.

Fernando, S., Gunasekara, C., Law, D.W., Nasvi, M.C.M., Setunge, S., Dissanayake, R., 2022. Engineering properties of waste-based alkali activated concrete brick containing low calcium fly ash and rice husk ash: a comparison with traditional Portland cement concrete brick. J. Build. Eng. 46, 103810.
Gavric, S., Leonhardt, G., Marsalek, J., Viklander, M., 2019. Processes improving urban stormwater quality in grass swales and filter strips: a review of research findings. Sci. Total Environ. 669, 431–447.
Gu, S., Boase, E.M., Lan, C.Q., 2021. Enhanced Pb(II) removal by green alga Neochloris oleoabundans cultivated in high dissolved inorganic carbon cultures. Chem. Eng. J. 416.
Gupta, S., Kashani, A., 2021. Utilization of biochar from unwashed peanut shell in cementitious building materials - effect on early age properties and environmental benefits. Fuel Process. Technol. 218, 106841.
Gupta, S., Kua, H.W., Pang, S.D., 2020. Effect of biochar on mechanical and permeability properties of concrete exposed to elevated temperature. Construct. Build. Mater. 234, 117338.
Gupta, S., Kua, H.W., 2019a. Carbonaceous micro-filler for cement: effect of particle size and dosage of biochar on fresh and hardened properties of cement mortar. Sci. Total Environ. 662, 952–962.
Gupta, S., Kua, H.W., 2019b. Combination of biochar and silica fume as partial cement replacement in mortar: performance evaluation under normal and elevated temperature. Waste Biomass Valorization 11, 2807–2824.
Gupta, S., Kua, H.W., Koh, H.J., 2018a. Application of biochar from food and wood waste as a green admixture for cement mortar. Sci. Total Environ. 619–620, 419–435.
Gupta, S., Kua, H.W., Low, C.Y., 2018b. Use of biochar as carbon sequestering additive in cement mortar. Cem. Concr. Compos. 87, 110–129.
Herath, C., Gunasekara, C., Law, D.W., Setunge, S., 2020. Performance of high volume fly ash concrete incorporating additives: a systematic literature review. Construct. Build. Mater. 258, 120606.
Inyang, M.I., Gao, B., Yao, Y., Xue, Y., Zimmerman, A., Mosa, A., Pullammanappallil, P., Ok, Y.S., Cao, X., 2015. A review of biochar as a low-cost adsorbent for aqueous heavy metal removal. Crit. Rev. Environ. Sci. Technol. 46, 406–433.
Kayhanian, M., Li, H., Harvey, J.T., Liang, X., 2019. Application of permeable pavements in highways for stormwater runoff management and pollution prevention: California research experiences. Int. J. Transp. Sci. Technol. 8, 358–372.
Kayhanian, M., Stransky, C., Bay, S., Lau, S.L., Stenstrom, M.K., 2008. Toxicity of urban highway runoff with respect to storm duration. Sci. Total Environ. 389, 386–406.
Krishnan, A.K., Sreejalekshmi, K.G., Vimexen, V., Dev, V.V., 2016. Evaluation of adsorption properties of sulphurised activated carbon for the effective and economically viable removal of Zn(II) from aqueous solutions. Ecotoxicol. Environ. Saf. 124, 418–425.
Kumar, P.S., Gayathri, R., Rathi, B.S., 2021. A review on adsorptive separation of toxic metals from aquatic system using biochar produced from agro-waste. Chemosphere 285, 131438.
Kumara, G.M.P., Kawamoto, K., Saito, T., Hamamoto, S., Asamoto, S., 2019. Evaluation of autoclaved aerated concrete fines for removal of Cd(II) and Pb(II) from wastewater. J. Environ. Eng. 145 (11).
Ma, Y., Egodawatta, P., Mcgree, J., Liu, A., Goonetilleke, A., 2016. Human health risk assessment of heavy metals in urban stormwater. Sci. Total Environ. 557-558, 764–772.
Maljaee, H., Madadi, R., Paiva, H., Tarelho, L., Ferreira, V.M., 2021a. Incorporation of biochar in cementitious materials: a roadmap of biochar selection. Construct. Build. Mater. 283, 122757.
Maljaee, H., Paiva, H., Madadi, R., Tarelho, L.a.C., Morais, M., Ferreira, V.M., 2021b. Effect of cement partial substitution by waste-based biochar in mortars properties. Construct. Build. Mater. 301, 124074.
Mbui, D., Njomo, N., Gitita, M., Ndekei, A., 2021. Synthesis and characterization of rice husk biochar and its application in the adsorption studies of lead and copper. Int. Res. J. Pure. Appl. Chem. 36–50.
Mullaney, J., Lucke, T., 2014. Practical review of pervious pavement designs. Clean: Soil, Air, Water 42, 111–124.
Nguyen, T.C., Loganathan, P., Nguyen, T.V., Vigneswaran, S., Kandasamy, J., Naidu, R., 2015. Simultaneous adsorption of Cd, Cr, Cu, Pb, and Zn by an iron-coated Australian zeolite in batch and fixed-bed column studies. Chem. Eng. J. 270, 393–404.
Ofori-Boadu, A.N., Bryant, D., Bock-Hyeng, C., Assefa, Z., Aryeetey, F., Munkaila, S., Fini, E., 2021. Physiochemical characterization of agricultural waste biochars for partial cement replacement. Int. J. Build. Pathol. Adapt. 40 (4), 569–586.
Ok, Y.S., Yang, J.E., Zhang, Y.S., Kim, S.J., Chung, D.Y., 2007. Heavy metal adsorption by a formulated zeolite-Portland cement mixture. J. Hazard Mater. 147, 91–96.
Pan, X., Zuo, G., Su, T., Cheng, S., Gu, Y., Qi, X., Dong, W., 2019. Polycarboxylic magnetic polydopamine sub-microspheres for effective adsorption of malachite green. Colloids Surf. Physicochem. Eng. Aspects 560, 106–113.
Park, J.Y., Byun, H.J., Choi, W.H., Kang, W.H., 2008. Cement paste column for simultaneous removal of fluoride, phosphate, and nitrate in acidic wastewater. Chemosphere 70, 1429–1437.
Park, J.-H., Wang, J.J., Kim, S.-H., Cho, J.-S., Kang, S.-W., Delaune, R.D., Han, K.-J., Seo, D.-C., 2017. Recycling of rice straw through pyrolysis and its adsorption behaviors for Cu and Zn ions in aqueous solution. Colloids Surf. Physicochem. Eng. Aspects 533, 330–337.
Poo, K.-M., Son, E.-B., Chang, J.-S., Ren, X., Choi, Y.-J., Chae, K.-J., 2018. Biochars derived from wasted marine macro-algae (Saccharina japonica and Sargassum fusiforme) and their potential for heavy metal removal in aqueous solution. J. Environ. Manage. 206, 364–372.
Poursaee, A., 2016. Corrosion of steel in concrete structures. In: Poursaee, A. (Ed.), Corrosion of steel in concrete structures. Woodhead Publishing, Oxford, pp. 19–33.
Praneeth, S., Ruonan, G., Dubey, B., Sarmah, A., 2020. Accelerated carbonation of biochar reinforced cement-fly ash composites: enhancing and sequestering CO_2 in building materials. Construct. Build. Mater. 244, 118363.
Qi, X., Wei, W., Su, T., Zhang, J., Dong, W., 2018. Fabrication of a new polysaccharide-based adsorbent for water purification. Carbohydr. Polym. 195, 368–377.
Qin, Y., Pang, X., Tan, K., Bao, T., 2021. Evaluation of pervious concrete performance with pulverized biochar as cement replacement. Cem. Concr. Compos. 119, 104022.
Rasoulifard, M.H., Khanmohammadi, S., Heidari, A., 2016. Adsorption of cefixime from aqueous solutions using modified hardened paste of Portland cement by perlite; optimization by Taguchi method. Water Sci. Technol. 74, 1069–1078.
Reddy, K.R., Xie, T., Dastgheibi, S., 2014. Removal of heavy metals from urban stormwater runoff using different filter materials. Journal of Environmental Chemical Engineering 2, 282–292.
Roy, K., Akhtar, A., Sachdev, S., Hsu, M., Lim, J., Sarmah, A., 2017. Development and characterization of novel biochar-mortar composite utilizing waste derived pyrolysis biochar. Int. J. Sci. Eng. Res. 8 (12).
Sakson, G., Brzezinska, A., Zawilski, M., 2018. Emission of heavy metals from an urban catchment into receiving water and possibility of its limitation on the example of Lodz city. Environ. Monit. Assess. 190, 281.
Saleh, T.A., 2015. Nanocomposite of carbon nanotubes/silica nanoparticles and their use for adsorption of Pb(II): from surface properties to sorption mechanism. Desalination Water Treat. 57, 10730–10744.
Šavija, B., Luković, M., 2016. Carbonation of cement paste: understanding, challenges, and opportunities. Construct. Build. Mater. 117, 285–301.
Shen, Z., Zhang, Y., Jin, F., Mcmillan, O., Al-Tabbaa, A., 2017. Qualitative and quantitative characterisation of adsorption mechanisms of lead on four biochars. Sci. Total Environ. 609, 1401–1410.
Shin, S., Jang, J., Yoon, S.H., Mochida, I., 1997. A study on the effect of heat treatment on functional groups of pitch based activated carbon fiber using FTIR. Carbon 35, 1739–1743.
Sidhu, V., Barrett, K., Park, D.Y., Deng, Y., Datta, R., Sarkar, D., 2020. Wood mulch coated with iron-based water treatment residuals for the abatement of metals and phosphorus in simulated stormwater runoff. Environ. Technol. Innov. 21, 101214.
Tan, K., Pang, X., Qin, Y., Wang, J., 2020. Properties of cement mortar containing pulverized biochar pyrolyzed at different temperatures. Construct. Build. Mater. 263, 120616.
Sun, C., Chen, T., Huang, Q., Wang, J., Lu, S., Yan, J., 2019. Enhanced adsorption for Pb (II) and Cd(II) of magnetic rice husk biochar by KMnO4 modification. Environ. Sci. Pollut. Res. Int. 26, 8902–8913.
Tan, X., Liu, Y., Zeng, G., Wang, X., Hu, X., Gu, Y., Yang, Z., 2015. Application of biochar for the removal of pollutants from aqueous solutions. Chemosphere 125, 70–85.
Wang, Y., Liu, R., 2017. Comparison of characteristics of twenty-one types of biochar and their ability to remove multi-heavy metals and methylene blue in solution. Fuel Process. Technol. 160, 55–63.
Wang, J., Zhao, Y., Yang, L., Tu, N., Xi, G., Fang, X., 2017. Removal of heavy metals from urban stormwater runoff using bioretention media mix. Water 9 (11).
Tchounwou, P.B., Yedjou, C.G., Patlolla, A.K., Sutton, D.J., 2012. Heavy metal toxicity and the environment. Exp. Suppl. 101, 133–164.
USEPA, 2014. National Recommended Water Quality Criteria Tables [Online]. Office of Science and Technology. https://www.epa.gov/wqc/national-recommended-water-quality-criteria-human-health-criteria-table. (Accessed 2 January 2021).
Wang, L., Chen, L., Tsang, D.C.W., Guo, B., Yang, J., Shen, Z., Hou, D., Ok, Y.S., Poon, C. S., 2020. Biochar as green additives in cement-based composites with carbon dioxide curing. J. Clean. Prod. 258, 120678.
Wijeyawardana, P., Nanayakkara, N., Gunasekara, C., Karunarathna, A., Law, D., Pramanik, B.K., 2022a. Improvement of heavy metal removal from urban runoff using modified pervious concrete. Sci. Total Environ. 815, 152936.
Wijeyawardana, P., Nanayakkara, N., Gunasekara, C., Karunarathna, A., Law, D., Pramanik, B.K., 2022b. Removal of Cu, Pb and Zn from stormwater using an industrially manufactured sawdust and paddy husk derived biochar. Environ. Technol. Innov. 28, 102640.
Xu, Z., Lin, Y., Lin, Y., Yang, D., Zheng, H., 2021. Adsorption behaviors of paper mill sludge biochar to remove Cu, Zn and As in wastewater. *Environ. Technol. Innov.,* 23.
Yang, X., Lin, R.S., Han, Y., Wang, X.Y., 2021. Behavior of biochar-modified cementitious composites exposed to high temperatures. Materials 14 (18).
Yankovych, H., Novoseltseva, V., Kovalenko, O., Marcin Behunova, D., Kanuchova, M., Vaclavikova, M., Melnyk, I., 2021. New perception of Zn(II) and Mn(II) removal mechanism on sustainable sunflower biochar from alkaline batteries contaminated water. J. Environ. Manage. 292, 112757.
Yoshida, T., Yamaguchi, T., Iida, Y., Nakayama, S., 2003. XPS Study of Pb (II) Adsorption on γ-Al_2O_3 surface at high pH conditions. J. Nucl. Sci. Technol. 40, 672–678.
Zhao, S., Ta, N., Wang, X., 2020. Absorption of Cu(II) and Zn(II) from aqueous solutions onto biochars derived from apple tree branches. Energies 13, 3498.
Zhou, Z., Xu, Z., Feng, Q., Yao, D., Yu, J., Wang, D., Lv, S., Liu, Y., Zhou, N., Zhong, M.-E., 2018. Effect of pyrolysis condition on the adsorption mechanism of lead, cadmium and copper on tobacco stem biochar. J. Clean. Prod. 187, 996–1005.
Zuraini, N.A., Alias, N., Mohamed Yusof, Z., Hanapi, M.N., Harun, S., 2018. First flush analysis of urban stormwater runoff from an urban catchment in Johor, Malaysia. MATEC Web of Conferences 250, 06014.